nature photonics
SUPPLEMENTARY INFORMATION
DOI: 10.1038/NPHOTON.2014.270

High-throughput imaging of heterogeneous cell organelles with an X-ray laser

SUPPLEMENTARY MATERIALS

Max F. Hantke[1*], Dirk Hasse[1*], Filipe R. N. C. Maia[1,2], Tomas Ekeberg[1], Katja John[1], Martin Svenda[1], N. Duane Loh[3], Andrew V. Martin[4], Nicusor Timneanu[1], Daniel S. D. Larsson[1], Gijs van der Schot[1], Gunilla H. Carlsson[1], Margareta Ingelman[1], Jakob Andreasson[1], Daniel Westphal[1], Mengning Liang[5], Francesco Stellato[5,6], Daniel P. DePonte[7], Robert Hartmann[8], Nils Kimmel[9], Richard A. Kirian[5], M. Marvin Seibert[1,7], Kerstin Mühlig[1], Sebastian Schorb[7], Ken Ferguson[7], Christoph Bostedt[7], Sebastian Carron[7], John D. Bozek[7], Daniel Rolles[5], Artem Rudenko[10], Sascha Epp[5], Henry N. Chapman[5], Anton Barty[5], Janos Hajdu[1,11] & Inger Andersson[1]

[1] Laboratory of Molecular Biophysics, Department of Cell and Molecular Biology, Uppsala University, Husargatan 3 (Box 596), SE-751 24 Uppsala, Sweden.

[2] NERSC, Lawrence Berkeley National Laboratory, Berkeley, California, USA.

[3] Centre for BioImaging Sciences, National University of Singapore, 14 Science Drive 4, Singapore 117557, Singapore.

[4] ARC Centre of Excellence for Coherent X-ray Science, School of Physics, The University of Melbourne, Victoria, 3010, Australia.

[5] Center for Free-Electron Laser Science, DESY, Notkestrasse 85, 22607 Hamburg, Germany.

[6] I.N.F.N. and Physics Department, University of Rome ‘Tor Vergata’, Via della Ricerca Scientifica 1, 00133, Rome, Italy.

[7] LCLS, SLAC National Accelerator Laboratory, 2575 Sand Hill Road, Menlo Park, California 94025, USA.

[8] PNSensor GmbH, Römerstrasse 28, 80803 München, Germany.

[9] Max Planck Institute for Extraterrestrial Physics, Giessenbachstrasse, 85741 Garching, Germany.

[10] Department of Physics, Kansas State University, 331 Cardwell Hall, Manhattan, Kansas 66506, USA.

[11] European XFEL GmbH, Albert-Einstein-Ring 19, 22761 Hamburg, Germany.

* These authors contributed equally to this project

Corresponding author: Janos Hajdu, janos@xray.bmc.uu.se

DOI: 10.1038/NPHOTON.2014.270

Section 1: Detection of multiple hits

Spatially separated particles with similar sizes give rise to diffraction patterns that can be similar to single particle diffraction patterns. Such patterns will pass the first filter as their central speckle can be approximated with a spheroid model. We identified these multiple hits from the presence of cross-terms in the autocorrelation. The autocorrelation was obtained by Fourier transforming the intensity pattern. Masked-out pixels were filled in with intensity estimates from the spheroid model. In the autocorrelation domain, rows and columns were normalised by their median value to enhance contrast in the cross-terms and to suppress pixel correlations related to the read-out process of the detector. Finally, normalising the values radially by the median value, suppressed ringing in the vicinity of the self-terms. In the resulting image, the number of pixels that exceeded an empirically defined threshold was used as a score to discriminate multiple hits from single particle hits.

Section 2: Retrieval of particle size and hit intensity.

We estimated the particle diameter from the semi-diameters of the spheroid fitted to the pattern as $d=2(2a+c)/3$. We assumed that the particles had an electron density 0.322 $Å^{-3}$ corresponding to an atomic composition $H_{23}C_3NO_{10}S$ and a density of 1 g/cm^3 (ref. 2), and used these values to obtain the hit intensity for each particle. Centre coordinates of the pattern were determined by finding the position, which best fulfils Friedel's symmetry (this is a valid assumption for particles smaller than 210 nm along the direction of the X-ray beam at 1.131 nm wavelength). Out-of-plane rotations were unconstrained by the measurements. We constrained the rotational freedom of the particles to in-plane rotations because most of our particles were more or less spherical or only slightly elongated. Finally, we estimated the free parameters by non-linear least square regression using the Levenberg–Marquardt algorithm.

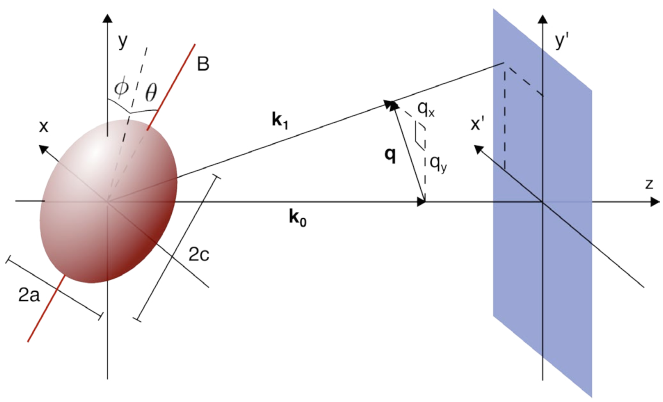

Supplementary Figure 1 | Diffraction geometry for a spheroid. The freely oriented spheroid with the semidiameters *a* and *c* is placed in the object plane. B denotes the body-axis. The diffraction intensity of the object is measured in the detector plane at a point defined by the scattering vector **q**.

We refer to the formula from Hamzeh[46] for small-angle far-field diffraction from a uniform spheroid. The spheroid is an ellipsoid of revolution whose shape is described by the two parameters *a* and *c* denoting the semi-diameters orthogonal to and along the axis of revolution, respectively (Supplementary Fig. 1). Two Euler angles θ and ϕ describe the orientation by consecutive rotation with respect to the x-axis (out-of-plane rotation) and the z-axis (in-plane rotation). For scattered photons of wavelength λ the intensity distribution $I(q)$ can be expressed by a function of the transversal components q_x and q_y of the scattering vector $\boldsymbol{q}=\boldsymbol{k}_1-\boldsymbol{k}_0$ with $|k_0|=|k_1|=2\pi/\lambda$.

$$I(\boldsymbol{q}) = S \cdot r_0^2 \Omega \cdot \left(\frac{4}{3}\pi a^2 c\right)^2 \cdot \left[\frac{3\cdot(\sin(qH(\boldsymbol{q})) - qH(\boldsymbol{q})\cdot\cos(qH(\boldsymbol{q})))}{(qH(\boldsymbol{q}))^3}\right]^2,$$

where S is a scaling factor, r_0 denotes the classical electron radius, Ω denotes the solid angle of integration, $H(\mathbf{q}) = \sqrt{a^2 \sin^2 g(\mathbf{q}) + c^2 \cos^2 g(\mathbf{q})}$ and $g(\mathbf{q}) = \frac{q_y \cos\theta\cos\phi - q_x \cos\theta \sin\phi}{q^2}$. The scaling factor $S=I_0\rho_e^2$ depends on two quantities, the intensity I_0 of the incoming wave ("hit intensity") and the electron density $\rho_e=0.322$ Å^{-3} of the particle.

Section 3: Fourier ring correlation and image splitting

We calculate the Fourier ring correlation (FRC, refs. 40-43) to guard against over-fitting our reconstructions to noise. FRC is calculated from two independent reconstructions extracted from the same diffraction pattern as shown in Supplementary Fig. 2. We divided the pixels of each pattern into two sets by going through every super-pixel (i.e. set of native pixels to be combined to a down-sampled pixel) and selecting 8 pixels at random, which we then averaged and assigned to the first image. We then averaged the remaining pixels and assigned the values to the second image. In the end the two reconstructed images are 4-times down-sampled versions of the starting reconstructions and their source pixels are independent and complementary.

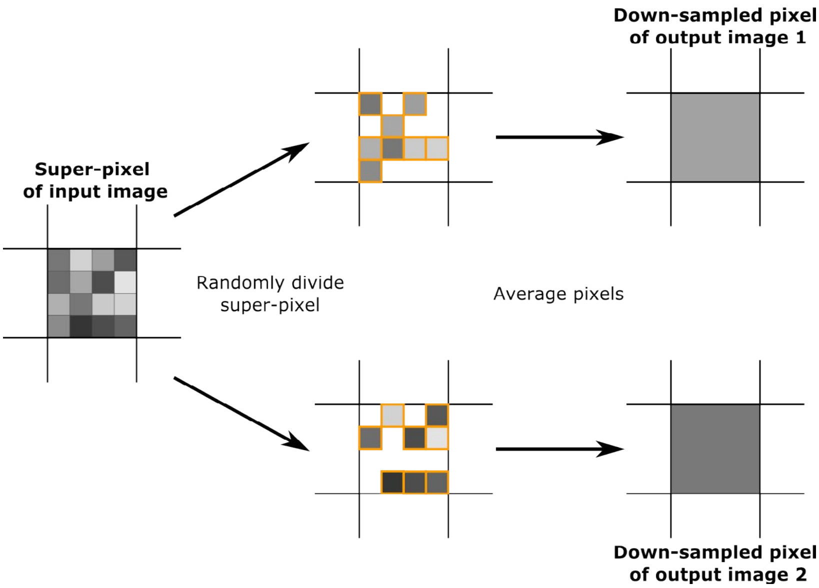

Supplementary Figure 2 | Image splitting for Fourier ring correlation.

We used the following algorithm to obtain 2 independent images from the same diffraction pattern (Supplementary Fig. 2):

1. Divide the input image into 4x4 super-pixels.

DOI: 10.1038/NPHOTON.2014.270

2. For each of the super-pixels select 8 pixels at random.

3. Average the selected pixels and assign the result to the corresponding down-sampled pixel in output image 1.

4. Average the remaining 8 pixels (those not selected in step 3) and assign the result to the corresponding down-sampled pixel in output image 2.

Supplementary references

40. Saxton, W. O. & Baumeister, W. The correlation averaging of a regularly arranged bacterial cell envelope protein. *J. Microscopy* **127**, 127–138 (1982).

41. van Heel, M., Keegstra, W., Schutter, W., & van Brüggen E. F. J. *Arthropod Hemocyanin Studies by Image Analysis, in: Structure and Function of Invertebrate Respiratory Proteins*. EMBO Workshop 1982, E. J. Wood. *Life Chemistry Reports*. Suppl. 1. pp. 69–73 (1982).

42. van Heel, M. & Schatz, M. Fourier shell correlation threshold criteria. *J. Struct. Biol.* **151**, 250–262 (2005).

46. Hamzeh, F. M. & Bragg, R. H. Small angle scattering of x-rays from groups of nonrandomly oriented ellipsoids of revolution of low concentration. *J. Appl. Phys.* **45**, 3189-3195 (1974).